Nano Energy 110 (2023) 108347

Contents lists available at ScienceDirect

Nano Energy

journal homepage: www.elsevier.com/locate/nanoen

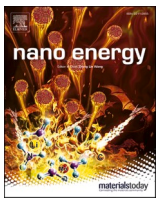

Triboelectric polymer with excellent enhanced electrical output performance over a wide temperature range

Shaowei Shen [a,b,1], Yangjiu Zhao [a,1], Ruirui Cao [a,*], Haoyi Wu [a], Weifeng Zhang [a], Yuxuan Zhu [b], Kailiang Ren [b,c], Caofeng Pan [b,c,**]

[a] Henan Key Laboratory of Photovoltaic Materials, Henan University, Kaifeng 475004, PR China
[b] CAS Center for Excellence in Nanoscience, Beijing Key Laboratory of Micro-nano Energy and Sensor, Beijing Institute of Nanoenergy and Nanosystems, Chinese Academy of Sciences, Beijing 101400, PR China
[c] School of Nanoscience and Technology, University of Chinese Academy of Sciences, Beijing 100049, PR China

ARTICLE INFO

Keywords:
Polymer tribomaterials
Fatty acid
Triboelectric nanogenerator
High temperature
Enhanced electrical output
Stability

ABSTRACT

Due to thermionic emission of triboelectric charge and degradation of mechanical stability of polymer tribomaterials (PTMs), PTMs based TENG (PTM-TENG) cannot maintain efficient electrical output and operate stably at high temperatures. Herein, a series of fatty acid doped PVDF-HFP (PH-FA) PTMs are fabricated. The introduction of FA lubricants dramatically increases the β-phase relative fraction, dielectric constant and surface charge potential of PTMs. Therefore, the PH-SA (stearic acid) based TENG shows improved electrical output over a wide temperature range, extraordinary stability, and durability. Particularly, the V_T/V_{Room}, I_T/I_{Room} and Q_T/Q_{Room} of PH-SA at 100 °C are separately up to 231.10%, 251.46% and 234.01%, the output efficiency of PH-SA is still higher than 100% at 120 °C. This study not only provides pioneering reference for the development of advanced PTM-TENG with enhanced output performance over a wide temperature range, but also greatly promotes the application of PTM-TENG devices in harsh environments.

1. Introduction

With the rapid development of the information age and the Internet of Things (IoT), triboelectric nanogenerator (TENG) has attracted extensive interests and shows great application potential because it can effectively convert tiny mechanical energy into high-performance electric power supply for portable and wearable electronic devices [1]. Continuous improvements to the output performance of TENG is the driving force for its ongoing development. TENG is known to basically manufactured by using two tribomaterials with different electron capture capabilities to generate electricity through the conjugation of contact electrification (CE) and electrostatic induction effects [2–4]. Possessing the merits of diversity of material selection, excellent flexibility, machinability, stretchability, extensibility and light weight compared to classic metal and inorganic tribomaterials [5], polymer tribomaterials (PTMs) have thus undoubtedly become the core foundation of TENG technology.

To date, many research efforts have been devoted to improving the output performance of PTMs based TENG (PTM-TENG) from various perspectives (i.e., appropriate micro/nano structure manufacturing and surface chemical modification) [6]. However, the service lifetime, stability and robustness of PTM-TENG are facing challenges owing to the wearing and surface degradation [7–9]. With this, Wang and Yang et al. [10,11] severally reported oleic acid (OA) enhanced polystyrene (PS) based TENG and stearic acid (SA) enhanced polyvinyl chloride (PVC) based TENG with high output performance and low wear rate. In these studies [10,11], OA and SA were used to improve the electronegativity of PS and PVC separately, and as lubrication additives to reduce friction coefficient and wear. Shi and Li et al. [7,12] introduced hexadecane and squalane liquid lubricants into the friction interface of PTM-TENG individually, and the relevant research results show that this liquid lubrication strategy is able to inhibit wear and transfer of PTMs, avoid the formation of transfer film, increase the effective solid-solid contact area, squeeze the air at the friction interface, and capture more

* Corresponding author.
** Corresponding author at: CAS Center for Excellence in Nanoscience, Beijing Key Laboratory of Micro-nano Energy and Sensor, Beijing Institute of Nanoenergy and Nanosystems, Chinese Academy of Sciences, Beijing 101400, PR China.
E-mail addresses: rrcao0403@vip.henu.edu.cn (R. Cao), cfpan@binn.cas.cn (C. Pan).
[1] S. Shen and Y. Zhao contributed equally

https://doi.org/10.1016/j.nanoen.2023.108347
Received 15 January 2023; Received in revised form 10 March 2023; Accepted 11 March 2023
Available online 13 March 2023

transferred electrons, thus giving rise to higher electric outputs. However, previous studies are mostly carried out under a single external environment, ignoring the influence of environmental inconstancy (such as temperature) on the output performance of PTM-TENG.

It is well known that, due to thermionic emission effect, the electrons transferred to the surface of PTMs can be released into the vacuum after CE, resulting in the inability of PTM-TENG to maintain effective electrical output at high-temperature conditions [13–15]. Furthermore, the high-temperature working environments can further aggravate the wear and transfer of PTMs, promote the formation of transfer film [16], and make the PTMs lose their mechanical stability, which is bound to further reduce the effective output power of PTM-TENG [12,13]. In this case, the application of PTM-TENG in high-temperature environments, such as oil and gas wells, airplane's engines, automobile exhaust pipes, thermal power filed, ceramic and glass manufacturing, is bound to be severely limited [13,14,17]. The oil drilling industry, for example, needs to continuously monitor the vital safety and environmental parameters in extraction wells to prevent disasters such as oil spill, oil fire or eventual explosion [17]. While the IoT revolution is connecting billions of sensors that provide a fathomless amount of data, all these devices still need one thing: electricity [18,19]. However, current mechanical energy harvesting technology can not well deal with the extreme conditions encountered in oil and gas wells operating at high temperatures (up to 120 °C). Recently, a series of relevant works have been reported for improving the working temperature of PTM-TENG [13,15,17,20–22]. While these PTM-TENG can work stably at high temperatures, their electrical output is significantly lower than that at room temperature due to the persistent thermionic emission effect [13,15,17,20–22]. For example, PTM-TENG based on polytetrafluoroethylene (PTFE) can only maintain partial efficiency at high-temperature environments (86.21% at 120 °C) [16]. The output efficiency of PTM-TENGs based on PTFE-coated cotton fabric/flame-retardant silver-coated cotton fabric [15], polyimide (synthesized from 4,4′-(hexafluoroisopropylidene) phthalic anhydride and 2,2″-bis(trifluoromethyl)benzidine) [13], and polydimethylsiloxane can only maintain 62.64% (at 120 °C), 52.12% (at 120 °C), and 89.61% (at 100 °C), respectively. Worse, the output efficiency of PTM-TENG based on polystyrene [10] and PTFE [17] can separately only maintain 11.42% at 100 °C and 63.24% at 70 °C. Therefore, to ensure PTM-TENG possess enhanced output performance over a wide temperature range and to operate efficiently and long-term stably in the changing or harsh environments is an urgent problem to be solved for its effective application in high-temperature environments.

Considering these aspect, in this study, a series of fatty acid (FA) doped poly (vinylidene fluoride-co-hexafluoropropylene) (PVDF-HFP) (PH-FA) PTM films were successfully fabricated by blade coating technology and proper ratio optimization. Fatty acids are considered to be one of the classical boundary lubrication additives [20]. Here, the FA was used to improve the electronegativity of PVDF-HFP PTM, and meanwhile, used as lubrication additives to improve the wear resistance property. Once the operating ambient temperature of PH-FA based TENG exceeds the melting temperature of FA, the FA will change from solid state to liquid state. As mentioned above [7,12], the presence of liquid FA lubricants can also inhibit wear and transfer of PTMs to a certain extent, avoid the formation of transfer film, increase the effective solid-solid contact area, and capture more transferred electrons, so as to produce higher electric outputs, which makes it possible to construct PTM-TENG with enhanced output performance over a wide temperature range and efficient and long-term stable operation in changing or harsh high-temperature environments. The results show that all as-fabricated PH-FA based TENGs possess an excellent enhanced electrical output. The power density at room temperature increases by about 12.64 times from 133 mW/m^2 (PH based TENG) to 1681 mW/m^2 (PH-3.0CA based TENG, capric acid). More importantly, the PH-SA PTM still shows excellent enhanced electrical output characteristics, and the value of V_T/V_{Room}, I_T/I_{Room} and Q_T/Q_{Room} (output efficiency) at 100 °C are severally as high as 231.10%, 251.46% and 234.01%, which has not been reported in previous PTM-TENG related studies. Further, the output performance of PH-SA based TENG remains nearly unchanged during each continuous heating and cooling thermal cycle, before and after three continuous heating and cooling thermal cycles, and even at 100 °C high-temperature environment, which exhibit extraordinary stability, durability, and repeatability. Therefore, the PH-SA based TENG has an excellent amplified electrical output characteristics and extraordinary stability at high temperatures and over a wide temperature range. Moreover, the PH-CA and PH-SA based TENG can still maintain enhanced output performance at 120 °C compared with room temperature. The mechanism dominates the enhanced high-temperature electrical output performance was discussed and revealed in detail by a modified electron-cloud-potential-well model. This study not only creates a pioneering reference for the development of advanced PTM-TENG with enhanced output performance over a wide temperature range, but also supplies a strategy to harvest environmental energy in high-temperature environments, which greatly facilitates the application of TENG electronic devices in harsh environments.

2. Experimental section/methods

Fabrication of PH and PH-FA PTM films: Capric acid (CA) with different doping amount (i.e., 0.0, 0.5, 1.0, 1.5, 2.0, 3.0 and 5.0 wt%) was mixed with 9 g PVDF-HFP (Kynar 2500) and 36 g DMF/acetone (60 wt%/40 wt%) mixed solvents in a 50-mL sample flask. The solutions were stirred for 12 h at room temperature to make sure that PVDF-HFP was completely dissolved. The fabricated PVDF-HFP/CA solutions were blade coating on a flat pre-cleaning glass plane and then dried at 80 °C, as shown in Fig. 1A. After cooling down, the films were peeled off from glass plane, and the corresponding CA doped PVDF-HFP films (PH-CA PTM films) were marked as PH (pure PVDF-HFP film), PH-0.5CA, PH-1.0CA, PH-1.5CA, PH-2.0CA, PH-3.0CA and PH-5.0CA, respectively. Other fatty acids (i.e., octanoic acid, octadecanoic acid, lauric acid, palmitic acid, and stearic acid) doped PVDF-HFP films (PH-FA PTM films) with a doping amount of 3.0 wt% were fabricated by the same operation as above, and labeled as PH-OA, PH-ODA, PH-LA, PH-PA, and PH-SA, respectively.

Fabrication of PH and PH-FA based TENG: The PTM-TENGs (PH and PH-FA based TENG, 4.5 ×4.5 cm^2) were fabricated by layer-by-layer self-assemble technique, which are consist of an electronegative portion (PH-FA film), an electropositive portion (Cu) and a commercial Kapton (PI) film, and in which PI film was severally used as the support substrate and dielectric layer.

Characterization: Morphology of the samples was observed by emission scanning electron microscopy (Gemini SEM 500, ZEISS Company, Germany). Attenuated total reflectance-Fourier transform infrared (ATR-FTIR) measurement was used to analyze the crystal structure (β phase) conversion of PH-CA films. Thermal property and thermal stability of PVDF-HFP and fatty acids were evaluated with differential scanning calorimetry (DSC, DSC250, TA Instruments, USA) and thermogravimetric analyzer (TGA, TGA/DSC3 +, Mettler Toledo, Switzerland) at a rate of ± 10 °C min^{-1} and a heating rate of 10 °C min^{-1}, respectively. The output performance of PH-FA based TENG was measured by a high-impedance electrometer (Keithley 6514, USA) at an operating frequency of 1.5 Hz, and the film contact and the moving distance (10 mm) were controlled by a linear motor (TSMV120–1S). The contact area between Cu and PH or PH/FA film was 4.5 × 4.5 cm^2. The surface potential was measured by KPFM-mode AFM. KPFM images with an area of 5 × 5 μm^2 were scanned with 1 Hz scanning speed ambient condition. The dielectric spectroscopy was carried out using an impedance analyzer (4294 A, Agilent, USA) in the frequency range of 40 to 10^6 Hz.

3. Results and discussion

Fig. 1 A displays the detailed fabrication process of PH-FA films.

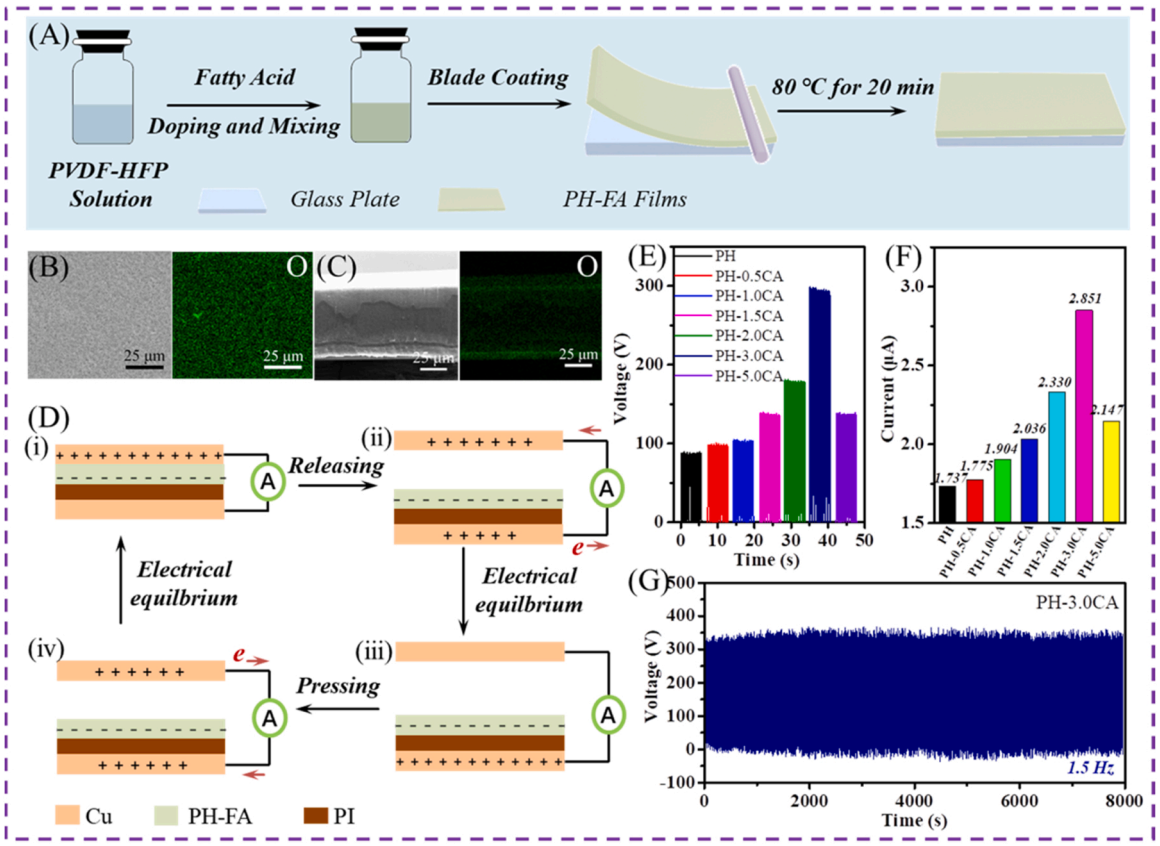

Fig. 1. Fabrication process, materials characterization and triboelectric properties of PH-FA films. (A) Fabrication process of PH-FA films. (B) SEM image of the surface morphology and EDS elemental mapping image of PH-3.0CA film. (C) SEM image of the cross section and EDS elemental mapping image of FH-3.0CA film. (D) Schematic of working mechanism of the vertical contact-separation mode PH-FA based TENGs. (E) V_{oc}, and (F) I_{sc} of PH-CA based TENGs. (G) Stability and robustness measurement of PH-3.0CA based TENG.

Where, PVDF-HFP is used as the PTM matrix due to its excellent properties of flexibility, adequate mechanical strength and high chemical resistance. The uniform dispersion of filler within a polymer matrix is one of the critical points for yielding excellent output performance [23]. It is widely known that solution blending technology is frequently used to fabricate high-performance materials with better molecular chain dispersion [24], and blade coating technology has the characteristics of simple, easy operation and low cost. In this study, both the polymer matrix PVDF-HFP and the dopant fatty acids have good solubility in the DMF/acetone mixed solvents. Therefore, in this study, a series of PH-FA films with a thickness of 45 μm~65 μm (Fig. S1) were fabricated through simple solution blending and blade coating technologies. The energy-dispersive X-ray spectroscopy (EDS) mapping images of the surface and cross section of PH-3.0CA film are manifested in Figs. 1B-1 C and Figs. S2A-S2B, respectively, and the corresponding EDS spectra are exhibited individually in Figs. S2C-S2D. The above EDS images and spectra revealed the uniform distribution of O, F and C elements. Fig. 1D evinces the structure and working mechanism of PH-FA based TENGs with a vertical contact separation mode. These PTM-TENGs consist of two main elements, namely, an electronegative portion (PH-FA film) and an electropositive portion (Cu). Additionally, these PTM-TENGs also include a commercial PI film as a dielectric layer, which is attached between the bottom of PH-FA film and the top of conductive Cu tape. This is mainly because the existence of dielectric layer (PI film) can optimize the trap distribution, charge capture and storage capacity of tribomaterials, resulting in improved TENG output [25,26]. Moreover, the fundamental working mechanism of PH-FA based TENGs is founded on the conjugation of CE and electrostatic induction effects [2,3,27], see the Supporting Information for details.

As exhibited in Fig. 1E-1 F and Fig. S3, the output performance, i.e., output voltage (V_{oc}), short circuit current (I_{sc}) and transferred charge (Q_{sc}) of PH-CA based TENGs show an apparent tendency of increasing first and then decreasing with the increase of CA doping amount. When CA doping amount increases from 0 wt% to 3.0 wt%, V_{oc} increases by 3.36 times from 88 V to 296 V, and I_{sc} increases by 1.64 times from 1.737 μA to 2.851 μA. Similarly, Q_{sc} also attains the maximum value of 129.88 nC from 37.46 nC. Once CA doping amount exceeds 3.0 wt%, the output performance of PH-CA based TENGs show an obvious downward trend. This performance degradation may be due to the agglomeration of excessive CA, which reduces the capacitance of the composite film [28]. This result was also confirmed by measurements of dielectric constant and surface potential below. To further demonstrate the influence of CA on the output performance of PVDF-HFP based PTM-TENGs, the output power and power density of PH and PH-CA based TENGs were estimated as presented in Figs. S4A-S4B. It is worth mentioning that the power density increases by about 12.64 times from 133 mW/m^2 (PH based TENG) to 1681 mW/m^2 (PH-3.0CA based TENG). The above results state clearly that doping CA into PVDF-HFP is an efficacious way to improve the output performance of PVDF-HFP based PTM-TENGs, and the PH-3.0CA film has a stronger triboelectric abilities. The specific reasons why CA can enhance the triboelectric properties and output performance of PVDF-HFP based PTM-TENGs will be analyzed in detail in the subsequent sections. Moreover, the PH-CA based TENGs, taking the PH-3.0CA based TENG as an example, exhibit a transcendental mechanical stability, as shown in Fig. 1 G and Figs. S4C-S4D. It can operate continuously for more than 12000 cycles without attenuation of output performance, which illustrates that the PH-CA based TENGs have excellent durability and can be widely used in practical applications.

Theoretically, choosing suitable materials as triboelectric layers at

the top and bottom of the triboelectric series can generate the maximum output power [8,29,30]. That is, in a TENG, when the tribo-electropositive material remains fixed, the greater the electronegativity of tribo-electronegative material used, the higher its output performance. Therefore, in order to disclose the mechanism of doping CA to improve the triboelectric properties and output performance of PVDF-HFP based PTM-TENGs, the electronegativity of PH and PH-CA films was first studied by Kelvin probe force microscopy (KPFM), and the surface charge potential of PH and PH-CA films were studied. As shown in Fig. 2A-2B, the surface charge potential increases in negative direction from − 404 mV (PH film) to − 651 mV (PH-3.0CA film), and exhibits a similar trend as observed in the output results of PH-CA films.

Moreover, abundant studies have indicated that the inherent characteristics of tribomaterials determine the output performance of TENG [31]. Consequently, analyzing the inherent characteristics of PH and PH-CA films can help to explore the origin of output differences between them and deepen our understanding of the underlying mechanism. To distinctly explain the improvement of output performance of PH-CA films, there are two key mechanisms: the first is that the introduction of fatty acids (such as CA) dramatically increased the β-phase relative fraction in the fabricated PH-CA films. It is widely known that PVDF-HFP is a semicrystalline polymer with three main crystalline phases: nonpolar α-phase, electroactive all-polar β-phase and semi-polar γ-phase. Among the three crystalline phases of PVDF-HFP, the β-phase can generate highest surface tribo-charge density because it provides the highest dipolar moment per unit cell. Thus, the presence of β-phase with a higher proportion will heighten dipole alignment and polarization in the fabricated PH-CA films, leading to improve the output performance of PH-CA based TENGs. In this study, to determine the crystalline state of PH and PH-CA films, the corresponding ATR-FTIR spectra were revealed in Fig. 2C. Based on the above ATR-FTIR spectra data, the relative fraction of β-phase, $F(\beta)$, in PH and PH-CA films can be calculated via Beer-Lambert equation as shown below [31],

$$F(\beta) = \frac{X_\beta}{X_\alpha + X_\beta} \times 100\% \quad (1)$$

$$= \frac{A_\beta}{(K_\beta \div K_\alpha)A_\alpha + A_\beta} \times 100\% \quad (2)$$

$$\approx \frac{A_\beta}{1.26A_\alpha + A_\beta} \times 100\% \quad (3)$$

where, X_α and X_β are individually the crystalline fractions of α-phase and β-phase, A_α and A_β represent severally the absorbance intensity at 767 cm^{-1} and 837 cm^{-1}, and the values of K_α and K_β are separately 6.1 × 10^4 cm^2 mol^{-1} and 7.7 × 10^4 cm^2 mol^{-1} [31]. The corresponding calculated results were shown in Fig. 2D, from which it can be clearly found that the $F(\beta)$ of all PH-CA films is higher than that of pure PH film, and the $F(\beta)$ increases by about 47.30% from 46.89% (PH film) to 69.07% (PH-2.0CA film). Consequently, the above results can confirm the expected boost in the β-phase relative fraction due to the existence of dopant CA. However, the $F(\beta)$ of PH-2.0CA film is higher than that of PH-3.0CA film, which is slightly different from the variation trend of output performance of PH-CA films above. Therefore, to more accurately explain the higher electric output performance with PH-CA films, compared to PH film, this study turns to the second factor, namely dielectric constant.

The dielectric property, because it is associated with the capability in storing electric charges, is an important intrinsic characteristic of tribomaterials, which is closely related to the electrical output of TENG [16]. Relevant researches suggest that the electric output of TENG is positively proportional to the dielectric constant of tribomaterials during contact-separation process [32]. For this reason, the increase of dielectric constant can improve the charge trapping capability of tribomaterials and promote the generation of a displacement current inside tribo-pairs, [30] which can significantly enhance the surface charge

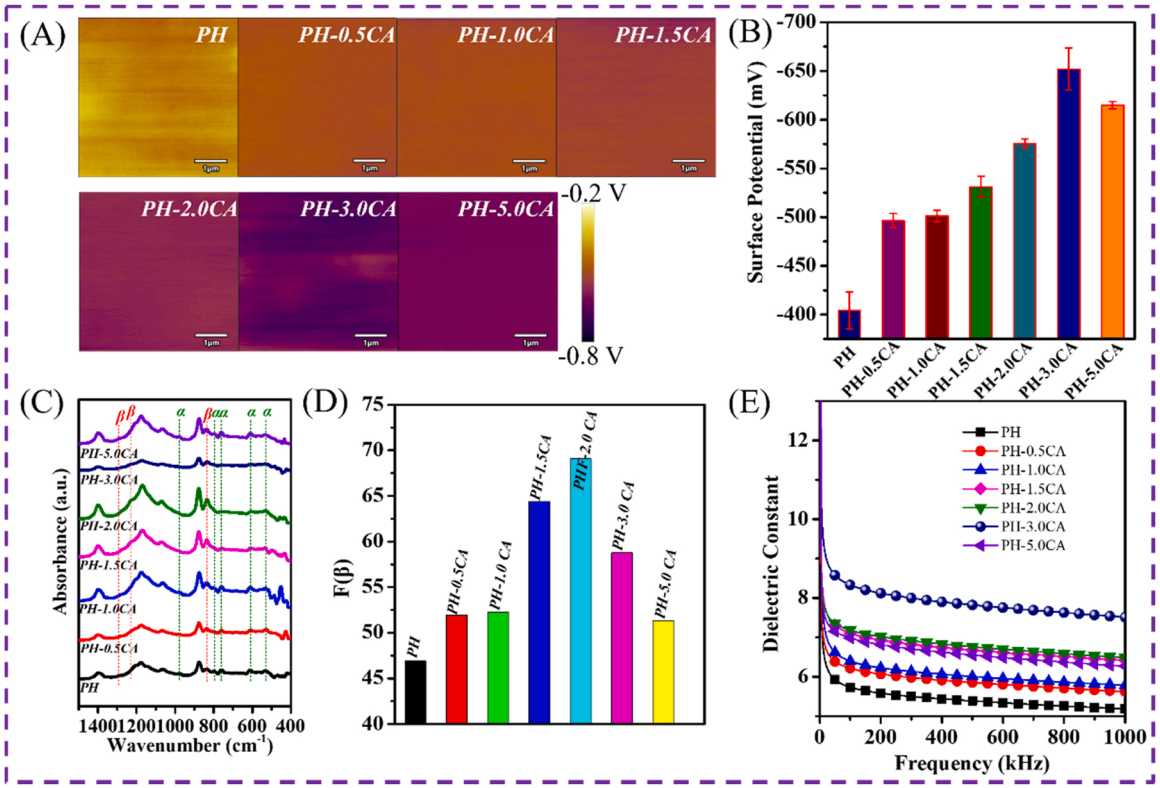

Fig. 2. Materials characterization for PH-CA films with different CA doping amount. Surface potential for (A) PH and (B) PH-CA composites with various CA doping amount. (C) ATR-FTIR spectra of PH-CA films. (D) The β phase content of PH-CA films. (E) Dependencies of dielectric constant value for PH-CA films.

density of tribo-layers, leading to a high electrical output of TENGs [33]. In this study, the dielectric constant (ε_r) of PH and PH-CA films from measured capacitance (C) is calculated according to the equation as given by [34],

$$\varepsilon_r = \frac{Cd}{\varepsilon_0 \times A} \tag{4}$$

where, d and A are the thickness and effective area of PH and PH-CA films, respectively, and the value of ε_0 is 8.85×10^{-12} F m^{-1}. The value of d herein is estimated from the cross-sectional micro-graphs of PH and PH-CA films, as illustrated in Fig. S1. As a result, the dielectric constant as function of frequency (F) ranging from 40–10^6 Hz for PH and PH-CA films were displayed in Fig. 2E and Fig. S5A. All the PH-CA films possessed a much higher dielectric constant than that of pure PH film, and the dielectric constant of PH-CA films increased with increasing CA doping amount up to 3.0 wt%, which exhibits a similar trend as observed in the electrical output results. Therefore, when the CA doping amount is 3.0 wt% in PH-CA films, the electrical output of PH-CA based TENGs reaches the maximum. Furthermore, the surface potential of tribo-layer is correlated with the β-phase relative fraction in PH-CA films and the dielectric constant of PH-CA films [35]. Apart from these, according to the relevant characterization results of SEM and AFM (Fig. S1 and Fig. S6), there is no significant difference in surface roughness and thickness of PH and PH-CA films. Consequently, according to the above characterization results, it can be concluded that the enhancement mechanism of PTM-TENG in this study is a combination of enhancing both dielectric constant and β-phase crystallinity.

Except CA, the effects of a series of other fatty acids (i.e., octanoic acid, octadecanoic acid, lauric acid, palmitic acid, and stearic acid, severally abbreviated as OA, ODA, LA, PA, and SA) with 3.0 wt% doping amount on the triboelectric output of PVDF-HFP were also studied, the corresponding test results were exhibited in Fig. 3A-3 C and Fig. S7. The fabricated PH-FA films herein were separately marked as PH-OA, PH-ODA, PH-LA, PH-PA and PH-SA films. Besides, the PH-3.0CA film thereinafter is represented by PH-CA film. From Fig. 3A-3 C and Fig. S7, it is clear that all PH-FA films possessed a much higher electrical output than that of pure PH film, which is consistent with the β-phase crystallinity ($F(\beta)$) of PH-FA films observed from Figs. S5B-S5C. Meanwhile, it again shows that it is an universal method to improve the triboelectric characteristics of PVDF-HFP based TENGs by doping fatty acids.

Generally, due to the thermionic emission of triboelectric charge and the degradation of mechanical stability of PTMs, the PTM-TENG cannot maintain effective electrical output under high-temperature conditions [13]. Namely, the electrical output of PTM-TENG is bound to be reduced at high-temperature operation environments [14,15]. Moreover, previous studies are mostly carried out at room temperature without considering the temperature effect on the electrical output of PTM-TENG, which is very critical for the application of electronics powered by PTM-TENG in different regions in the world [16]. Therefore, it is an urgent problem to ensure that PTM-TENG possesses enhanced output performance over a wide temperature range and works efficiently and stably in high-temperature (harsh, especially changing) environments [32]. Fig. S8 exhibits the DSC and TGA curves of PVDF-HFP and fatty acids, and the relevant DSC and TGA thermal properties are listed in Tables S1-S2, respectively. As displayed in Figs. S8A-S8C and Table S2, the melting temperature of PVDF-HFP is about 123 °C, and the PVDF-HFP is thermally stable up to nearly 450 °C, showing excellent thermal stability. From previous studies [36–39], it is known that the boiling point of fatty acids is between 230 ℃ and 380 ℃, among which the boiling point of SA is about 375 ℃ [37,38]. Meanwhile, as displayed in Fig. S8C, the fatty acids also have excellent thermal stability and the thermal resistance temperature of SA is up to 246 ℃. Additionally, as shown in Fig. S9, it can be confirmed that the PH-FA PTMs exhibit excellent thermal stability, thermal reliability, and structural stability.

To explore the electrical output of PH-FA films at high-temperature conditions, a series of PH-FA based TENGs were constructed. The structure and working mechanism of PH-FA based TENGs in this part and subsequent discussions were shown in Fig. S10. The corresponding test results are shown in Fig. 3D-3 F and Figs. S11-S15, respectively. From these figures, it can be observed intuitively that the electrical output of PH and PH-FA based TENGs could stay stable at each

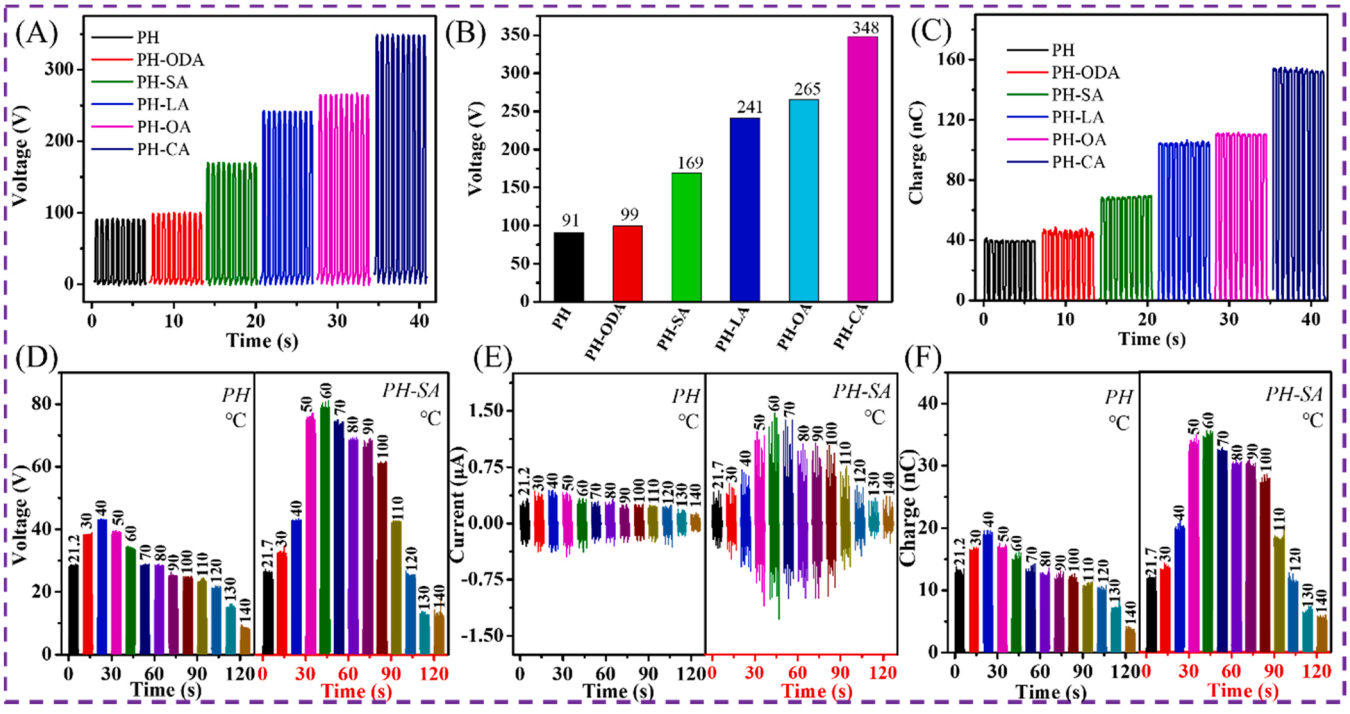

Fig. 3. Electrical output performance of vertical contact-separation mode PH and PH-FA based TENGs and temperature-dependent electrical output performance of PH and PH-SA based TENGs. (A) V_{oc}, (B) comparation by histogram of V_{oc} and (C) Q_{sc} of PH and PH-FA based TENGs. Temperature-dependent (D) V_{oc}, (E) I_{sc} and (F) Q_{sc} of PH and PH-SA based TENGs.

temperature point, and the V_{oc}, I_{sc} and Q_{sc} show an obvious tendency of increasing first and then decreasing with the increase of temperature, which is similar to the previously reported results [16]. There are three main reasons for the above tendency of increasing first and then decreasing: the first is that the hotter tribo-layer's electron energy levels will increase due to the raised temperature, and the electrons locating at a high energy level in the hotter tribo-layer will transit to its surface state, so as to more transferred electrons during friction to enhance the electrical output [14]. The second is that FA will change from solid state to liquid state with the increase of temperature, the existence of liquid FA can increase the effective solid-solid contact area, squeeze the air at the friction interface, and capture more transferred electrons, resulting in higher electric output [7,12]. The third is that the electron thermionic emission will be more intense with temperature increasing, which results in a decrease of charge density and electrical output of TENG [15,16,40]. Therefore, the competition of the increase of transferring charge and tribo-charge dissipation results in a complex changing tendency of the electrical output of PH and PH-FA based TENGs. Meanwhile, this behavior can be explained by electron-driving-related factors, which are affected during operating at high-temperatures [14]. An increase in temperature speeds up the electron transfer and introduces disorder, which is associated with the driving force of electron transfer from one layer to another, making better outputs at higher temperatures [20,41]. Nevertheless, very large thermal changes may overcome the barrier height, promote the backward electron transfer process, and degrade the output performance [20]. Therefore, there is an optimal temperature point to obtain the highest electrical outputs.

The normalized voltage (V_T/V_{Room}), normalized current (I_T/I_{Room}) and normalized charge (Q_T/Q_{Room}) (output efficiency) of PH and PH-FA based TENGs are shown in Fig. 4A-4 C and Fig. S16. Further, Fig. S17 provides the temperature-dependent V_{oc}, I_{sc} and Q_{sc} of PH and PH-SA films. As seen in Fig. S16, the PH-SA, PH-PA, PH-LA and PH-CA films all exhibit enhanced electrical output efficiency at high-temperature conditions, compared with pure PH film. In particular, the output efficiency of PH-CA and PH-SA is still higher than 100% at operating temperatures up to 120 °C, which is unprecedented. Therefore, compared to other PTM-TENG, the PH-FA (namely, PH-CA and PH-SA) based TENGs can be used to harvest mechanical energy from high-temperature objects more efficiency. Fig. 4A-4-C also shows the curves of V_T/V_{Room}, I_T/I_{Room} and Q_T/Q_{Room} of PH and PH-SA films as a function of temperature. It can be seen that PH-SA film still shows excellent enhanced electrical output characteristics over a wide temperature range, and even at 100 °C, the value of V_T/V_{Room}, I_T/I_{Room} and Q_T/Q_{Room} are as high as 231.10%, 251.46% and 234.01%, respectively, which have not been reported in previous PTM-TENG related studies. In addition, the variation trend between the output efficiency and temperature of as-fabricated PH-FA films is slightly different. Interestingly enough, recent studies have found that the introduction of proper liquid lubrication can not only provide a super wear-resistive TENG inhibiting wear and transfer of PTMs, but also can increase the electric output [7,10,12,42]. In this study, FAs are considered to be one of the classical boundary lubrication additives [20], the transformation of FA from solid to liquid mainly depends on the melting temperature of various FAs, and meanwhile, the viscosity and other physical parameters of fatty acids will inevitably change during this process. Therefore, the reason for this phenomenon may be the different melting points of dopant fatty acids. Except for enhanced electrical output characteristics, the high-temperature stability, durability and repeatability are also very important performance indexes in practical applications. To intuitively verify the high-temperature stability and durability of PH-FA film,

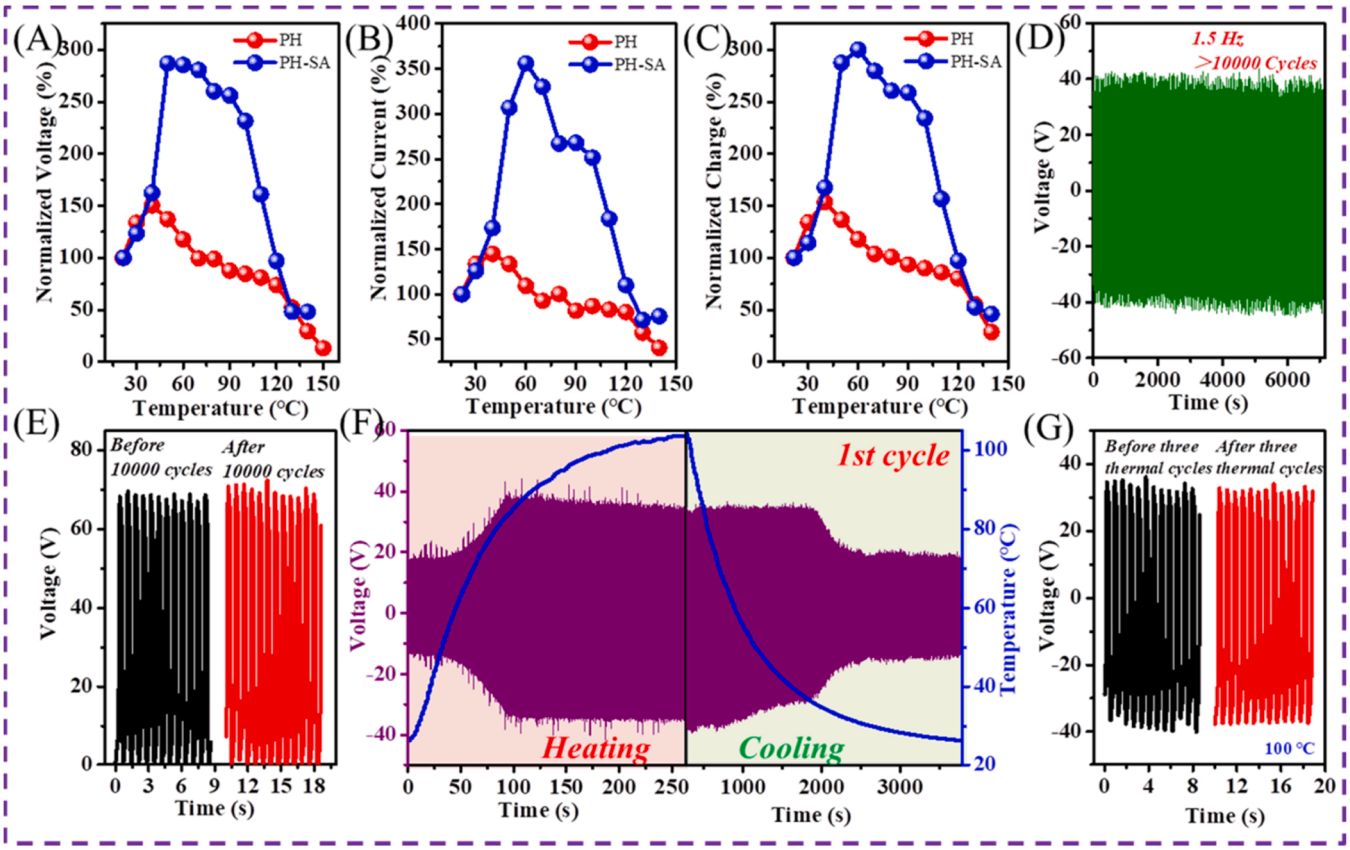

Fig. 4. Temperature-dependent electrical output performance of PH and PH-SA films. Normalized voltage (A), current (B) and charge (C) of PH and PH-SA films. (D) and (E) Stability and robustness measurement of PH-SA based TENG at 100 ℃. (F) V_{oc} of PH-SA based TENG during continuous heating and cooling. (G) V_{oc} comparation of PH-SA based TENG at 100 ℃ before and after three continuous heating and cooling thermal cycles.

taking the PH-SA film as an example, the V_{oc} of PH-SA based TENG was continuously measured at the frequency of 1.5 Hz. It is plain from Fig. 4D-4E that there is almost no drop in V_{oc} of PH-SA based TENG after more than 10000 cycles at an operating temperature of 100 °C. As shown in Fig. 4F-4 G and Fig. S18, the output performance of PH-SA based TENG remain nearly unchanged during each continuous heating and cooling thermal cycle and before and after three continuous heating and cooling thermal cycles. Additionally, Fig. S19 diplays the SEM micrographs of PH-SA film before and after continuous heating and cooling. From Fig. S19, the surface morphology of PH-SA film changed slightly before and after high temperature testing, and there was no obvious damage and crack, indicating that it has excellent mechanical stability and durability. To sum up, it can be confirmed that the PH-SA film exhibit outstanding high-temperature stability, durability and repeatability. More importantly, comparing Fig. 4F and Fig. S20, it is obvious that the output performance of PH based TENG decreases sharply with the increase of operating ambient temperature, while the output performance of PH-SA based TENG increases significantly, which also verifies once again that PH-SA film possesses enhanced electrical output characteristics over a wide temperature range and at high-temperature environments. As exhibited in Fig. S21-S23, PH-PA film and PH-CA film, like as PH-SA film, also has excellent high-temperature stability, durability and repeatability. Therefore, this study creates new possibilities for the development of advanced PTM-TENG with attractive characteristics and desirable performances, and promotes the application of TENG electronic devices in the changing or harsh environments such as oil and gas wells.

Since electrons in a general dielectrics do not have individual energy levels like in metals and semiconductors [43], the electron clouds and potential well model are presented as universal characteristics that all materials possess. Even in the presence of factors such as certain material characteristics at high temperatures that complicate dielectric CE studies, this model should also apply. Therefore, according to the newfound data on PH-SA based TENG at high temperatures, a modified electron-cloud-potential-well model (Fig. 5) is used to account for the electrons transfer process for CE between Cu and PH-SA tribo-layers at high temperatures [14,43,44]. Here, the transferred electrons and the electrons dissipated into the air by thermionic emission effect are represented by purple arrows and red arrows, respectively. And the electrons traveling through the circuit due to potential imbalance between the tribomaterials is demonstrated by blue arrows. As displayed in the left part of Fig. 5A-5B, the hotter tribo-layer's electron energy levels will increase ($\approx k\Delta T$) due to the raised temperature at high temperatures [14]. On one hand, electrons locating at a high energy level in the hotter tribo-layer will transit to its surface states, and more electrons will hop from Cu tribo-layer to PH and PH-SA tribo-layer, as shown in the middle part of Fig. 5A-5B, to enhance the charge density. On the other, because of electron thermionic emission effect of triboelectric charges, as the right part of Fig. 5A-5B exhibit, electrons are easier to escape out of the potential well and get back to the Cu tribo-layer or spill into the air (represent by the red arrows) at high temperatures, which reduces charge density and output performance of TENG. As a result, the competition of the increased transferring charge and triboelectric charge dissipation, results in a complex tendency of increasing first and then decreasing of the output performance of PH and PH-SA based TENGs with the increase of temperature. Last but most important, as shown in the middle and right parts of Fig. 5B, the presence of SA can improve the charge capture and storage capacity of PH-SA tribo-layer at high temperatures, resulting in the further increase of surface charge density and the weakening of triboelectric charge dissipation [10,12,32], so that the PH-SA based TENG has an excellent amplified electrical output characteristics at high temperatures and over a wide temperature range.

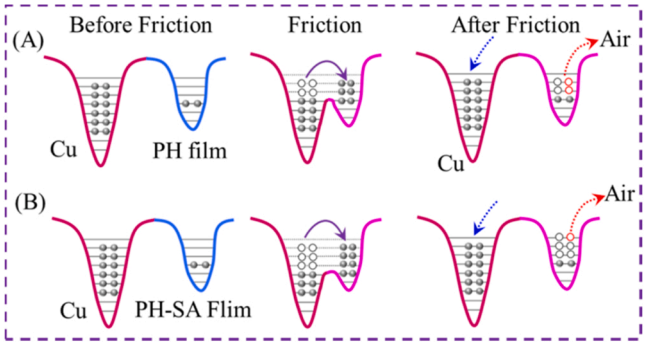

Fig. 5. The electrical output enhancement mechanism at high temperatures explained by electron-cloud-potential-well model. Contact electrification (CE), charge transfer and dissipation of (A) Cu and PH film, (B) Cu and PH-SA film at high temperatures, respectively.

To evaluate the charging capacity of PH-SA based TENG at different temperatures, a commercial capacitor (1 μF) was charged in the operating ambient temperature range from room temperature to 120 °C. Fig. S24 shows the schematic diagram of utilizing the PH-SA based TENG to charge the capacitor by a rectifier bridge. The corresponding results were shown in Fig. 6A-6B, it can clearly seen that the charging voltage of the capacitor at high temperatures is higher than that at room temperature, and shows an obvious tendency of increasing first and then decreasing with the increase of temperature, which is similar to the above electrical output results. It also verifies once again that the PH-SA based TENG has an excellent enhanced electrical output characteristics over a wide temperature and at high temperatures, which has hardly been reported in previous PTM-TENG related studies. Fig. 6C exhibits the comparison of output efficiency (χ, i.e., normalized voltage/current) of PH-SA based TENG in this study and those of previously reported similar studies. The relevant detailed data are also summarized in Table S3. As shown in Fig. 6C and Table S3, the χ values of PH-SA based TENG at various temperatures in present work are substantially higher than those of the TENGs at corresponding temperatures in previously reported similar studies [13,15–17,20–22,44,45]. And beyond that, as shown in Table S3, the electrical outputs of PH-SA based TENG at high temperatures are higher than or comparable to most of reported similar studies. Furthermore, compared to PH, the PH-SA based TENG can still light up 6 LEDs in a high-temperature operating ambient of about 100 °C, and the brightness of LEDs has no significant change compared with that at room temperature, as seen in Fig. 6D, Movie S1 and Fig. 6E, Movie S2, respectively. In conclusion, this PH-FA based TENG with excellent enhanced electrical output characteristics over a wide temperature and at high temperatures can be widely applied as the environmental energy harvester and self-powered sensor at extreme temperature environments [15,17,44,46–48], which includes the fire-fighting, forest fire alarm, oil drilling industry, thermal power filed, aerospace, automobile, gas extraction, steel, ceramic and glass manufacturing and other industrial fields in high-temperature environments.

Supplementary material related to this article can be found online at doi:10.1016/j.nanoen.2022.107777.

4. Conclusion

In summary, all PH-FA PTM films fabricated in this work possess an excellent enhanced electrical output. The power density at room temperature increases by about 12.64 times from 133 mW/m^2 (PH based TENG) to 1681 mW/m^2 (PH-3.0CA based TENG). In particular, the PH-CA, PH-PA and PH-SA based PTM-TENGs exhibit outstanding enhanced electrical output characteristics over a wide temperature and at high temperatures. Even at 100 °C, the value of V_T/V_{Room}, I_T/I_{Room} and Q_T/Q_{Room} of PH-SA film is still as high as 231.10%, 251.46% and 234.01%, respectively. Particularly, the output efficiency of PH-SA and PH-CA is still higher than 100% at 120 °C. Additionally, the PTM-TENG fabricated in this study also has extraordinary high-temperature stability, durability and repeatability. These results indicate that this study has

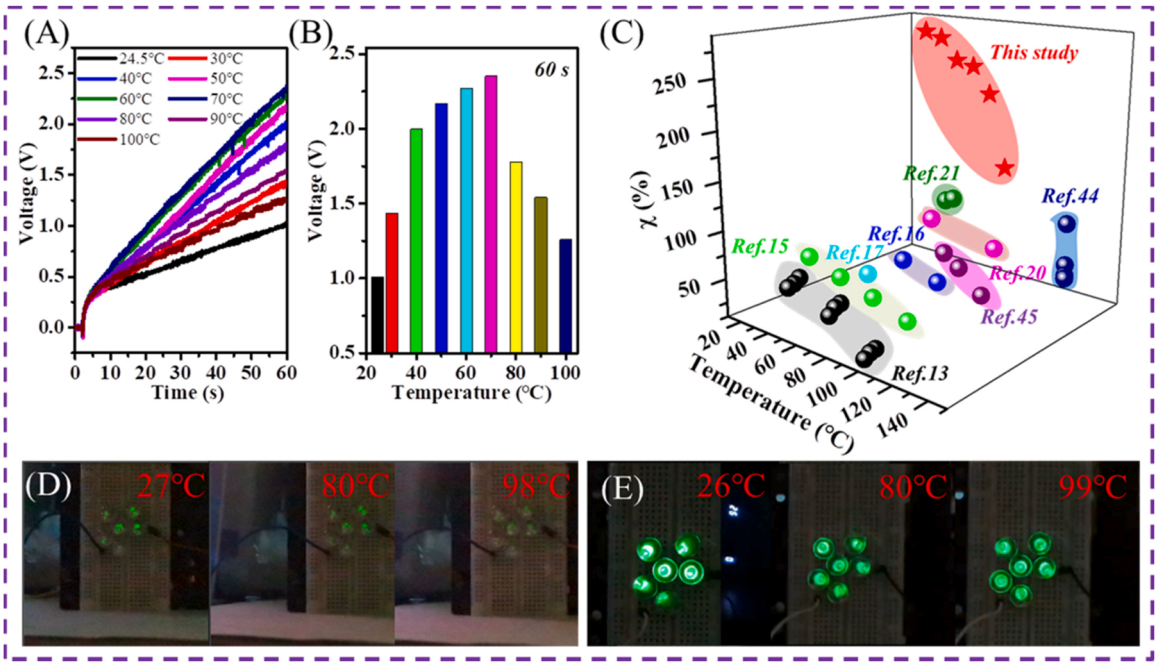

Fig. 6. Electrical output performance of PH and PH-SA based TENGs for various temperature states. (A) and (B) Charging performance of PH-SA based TENG to a capacitor of 1 μF. (C) Comparison of the χ of PH-SA film and those of previously reported similar studies. Photos of (D) PH and (E) PH-SA based TENGs to light 6 LEDs at different temperatures, respectively.

solved the bottleneck problem of the inability of PTM-TENG to maintain effective electrical output at high-temperature conditions. Compared to PH, the PH-SA based TENG can still light up 6 LEDs in a high-temperature operating ambient of about 100 °C, and the brightness of LEDs has no significant change compared with that at room temperature. Therefore, our finding fills the gap in the field of enhancing high-temperature electrical output PTM-TENG in the past. It not only creates a pioneering reference for the development of advanced PTM-TENG with enhanced electrical output characteristics over a wide temperature, but also supplies a more efficient strategy to harvest mechanical energy on high-temperature objects, which greatly promotes the application of PTM-TENG devices in extreme temperature environments.

CRediT authorship contribution statement

Shaowei Shen: Conceptualization, Methodology, Data collection and analysis. **Yangjiu Zhao**: Conceptualization, Methodology, Data collection and analysis. **Ruirui Cao**: Conceptualization, Methodology, Formal analysis, Discussion, Writing – original draft, Funding acquisition, Resources. **Haoyi Wu**: Data analysis. **Weifeng Zhang**: Supervision. **Yuxuan Zhu**: Data collection. **Kailiang Ren**: Data collection and analysis, Discussion. **Caofeng Pan**: Manuscript revision, Discussion, Supervision, Funding acquisition.

Declaration of Competing Interest

The authors declare that they have no known competing financial interests or personal relationships that could have appeared to influence the work reported in this paper.

Data Availability

Data will be made available on request.

Acknowledgements

This work was supported by the National Natural Science Foundation of China (No. 52003074, 52125205, U20A20166 and 52192614), the Project funded by China Postdoctoral Science Foundation (No. 2020M680097), the Natural Science Foundation of Henan Province (No. 202300410058), National key R&D program of China (2021YFB3200302 and 2021YFB3200304), Natural Science Foundation of Beijing Municipality (Z180011 and 2222088), Shenzhen Science and Technology Program (Grant No. KQTD20170810105439418) and the Fundamental Research Funds for the Central Universities.

Appendix A. Supporting information

Supplementary data associated with this article can be found in the online version at doi:10.1016/j.nanoen.2023.108347.

References

[1] D.W. Jin, Y.J. Ko, C.W. Ahn, S. Hur, T.K. Lee, D.G. Jeong, M. Lee, C.-Y. Kang, J. H. Jung, Polarization- and electrode-optimized polyvinylidene fluoride films for harsh environmental piezoelectric nanogenerator applications, Small 17 (2021), 2007289.
[2] Y. Park, Y.-E. Shin, J. Park, Y. Lee, M.P. Kim, Y.-R. Kim, S. Na, S.K. Ghosh, H. Ko, Ferroelectric multilayer nanocomposites with polarization and stress concentration structures for enhanced triboelectric performances, ACS Nano 14 (2020) 7101–7110.
[3] Z. Wang, W.L. Liu, W.C. He, H.Y. Guo, L. Long, Y. Xi, X. Wang, A.P. Liu, C.G. Hu, Ultrahigh electricity generation from low-frequency mechanical energy by efficient energy management, Joule 5 (2021) 441–455.
[4] Z.Q. Yuan, C.F. Wang, J.G. Xi, X. Han, J. Li, S.-T. Han, W.C. Gao, C.F. Pan, Spherical triboelectric nanogenerator with dense point contacts for harvesting multidirectional water wave and vibration energy, ACS Energy Lett. 6 (2021) 2809–2816.
[5] A.H. Chen, C. Zhang, G. Zhu, Z.L. Wang, Polymer materials for high-performance triboelectric nanogenerators, Adv. Sci. 7 (2020), 2000186.
[6] W.L. Liu, Z. Wang, C.G. Hu, Advanced designs for output improvement of triboelectric nanogenerator system, Mater. Today 45 (2021) 93–119.
[7] J. Wu, Y.H. Xi, Y.J. Shi, Toward wear-resistive, highly durable and high performance triboelectric nanogenerator through interface liquid lubrication, Nano Energy 72 (2020), 104659.
[8] Y.H. Liu, J.L. Mo, Q. Fu, Y.X. Lu, N. Zhang, S.F. Wang, S.X. Nie, Enhancement of triboelectric charge density by chemical functionalization, Adv. Funct. Mater. 30 (2020), 2004714.
[9] G. Ge, W. Yuan, W. Zhao, Y. Lu, Y.Z. Zhang, W.J. Wang, P. Chen, W. Huang, W. L. Si, X.C. Dong, Highly stretchable and autonomously healable epidermal sensor

based on multi-functional hydrogel frameworks, J. Mater. Chem. A 7 (2019) 5949–5956.
[10] J.J. Zhang, Y.B. Zheng, L. Xu, D.A. Wang, Oleic-acid enhanced triboelectric nanogenerator with high output performance and wear resistance, Nano Energy 69 (2020), 104435.
[11] H.J. Zhang, Y.L. Guo, H.D. Xu, G.R. Zhao, B.P. Yang, Stearic acid reinforced triboelectric nanogenerator with high output performance and anti-wear characteristics for self-powered anticorrosion system, Chem. Lett. 50 (2021) 844–848.
[12] K.Q. Wang, J.J. Li, J.F. Li, C.Y. Wu, S. Yi, Y.F. Liu, J.B. Luo, Hexadecane-containing sandwich structure based triboelectric nanogenerator with remarkable performance enhancement, Nano Energy 87 (2021), 106198.
[13] X.L. Tao, S.Y. Li, Y.X. Shi, X.L. Wang, J.W. Tian, Z.Q. Liu, P. Yang, X.Y. Chen, Z. L. Wang, Triboelectric polymer with high thermal charge stability for harvesting energy from 200 °C flowing air, Adv. Funct. Mater. 31 (2021), 2106082.
[14] B.L. Cheng, Q. Xu, Y.Q. Ding, S. Bai, X.F. Jia, Y.D.C. Yu, J. Wen, Y. Qin, High performance temperature difference triboelectric nanogenerator, Nat. Commun. 12 (2021) 4782.
[15] R.W. Cheng, K. Dong, L.X. Liu, C. Ning, P.F. Chen, X. Peng, D. Liu, Z.L. Wang, Flame-retardant textile-based triboelectric nanogenerators for fire protection applications, ACS Nano 14 (2020) 15853–15863.
[16] C.X. Lu, C.B. Han, G.Q. Gu, J. Chen, Z.W. Yang, T. Jiang, C. He, Z.L. Wang, Temperature effect on performance of triboelectric nanogenerator, Adv. Eng. Mater. 19 (2017), 1700275.
[17] C. Rodrigues, M. Kumar, M.P. Proenca, J. Gutierrez, R. Melo, A. Pereira, J. Ventura, Triboelectric energy harvesting in harsh conditions: temperature and pressure effects in methane and crude oil environments, Nano Energy 72 (2020), 104682.
[18] Q. Zhang, S.L. Zuo, P. Chen, C.F. Pan, Piezotronics in two-dimensional materials, InfoMat 3 (2021) 987–1007.
[19] C.F. Wang, R.H. Ma, D.F. Peng, X.H. Liu, J. Li, B.R. Jin, A.X. Shan, Y. Fu, L. Dong, W.C. Gao, Z.L. Wang, C.F. Pan, Mechanoluminescent hybrids from a natural resourcefor energy-related applications, InfoMat 3 (2021) 1272–1284.
[20] X.N. Wen, Y.J. Su, Y. Yang, H.L. Zhang, Z.L. Wang, Applicability of triboelectric generator over a wide range of temperature, Nano Energy 4 (2014) 150–156.
[21] S.A. Graham, S.C. Chandrarathna, H. Patnam, P. Manchi, J.-W. Lee, J.S. Yu, Harsh environment-tolerant and robust triboelectric nanogenerators for mechanical-energy harvesting, sensing, and energy storage in a smart home, Nano Energy 80 (2021), 105547.
[22] P.P. Zhang, Y.H. Chen, Z.H. Guo, W.B. Guo, X. Pu, Z.L. Wang, Stretchable, transparent, and thermally stable triboelectric nanogenerators based on solvent-free ion-conducting elastomer electrodes, Adv. Funct. Mater. 30 (2020), 1909252.
[23] Y.Z. Zhang, M.J. Wu, Q.Y. Zhu, F.Y. Wang, H.X. Su, H. Li, C.L. Diao, H.W. Zheng, Y. H. Wu, Z.L. Wang, Performance enhancement of flexible piezoelectric nanogenerator via doping and rational 3D structure design for self-powered mechanosensational system, Adv. Funct. Mater. 29 (2019), 1904259.
[24] X.F. Pan, J.J. Shi, Y.L. Jin, B.P. Liu, L.B. Li, X.L. He, Hierarchical structure manipulation of UHMWPE/HDPE fibers through in-reactor blending with Cr/V bimetallic catalysts, Compos. Sci. Technol. 175 (2019) 46–54.
[25] S.S. Lv, X. Zhang, T. Huang, H. Yu, Q.H. Zhang, M.F. Zhu, Trap distribution and conductivity synergic optimization of high-performance triboelectric nanogenerators for self-powered devices, ACS Appl. Mater. Inter. 13 (2021) 2566–2575.
[26] N.Y. Cui, L. Gu, Y.M. Lei, J.M. Liu, Y. Qin, X.H. Ma, Y. Hao, Z.L. Wang, Dynamic behavior of the triboelectric charges and structural optimization of the friction layer for a triboelectric nanogenerator, ACS Nano 10 (2016) 6131–6138.
[27] Y.X. Hu, X.Y. Li, Z.H. Zhao, C.G. Zhang, L.L. Zhou, Y.H. Li, Y.B. Liu, J. Wang, Z. L. Wang, Triboelectric nanogenerator with low crest factor via precise phase difference design realized by 3D printing, Small Methods 5 (2021), 2100936.
[28] B.B. Fan, G.X. Liu, X.P. Fu, Z.Z. Wang, Z. Zhang, C. Zhang, Composite film with hollow hierarchical silica/perfluoropolyether filler and surface etching for performance enhanced triboelectric nanogenerators, Chem. Eng. J. 446 (2022), 137263.
[29] H.Y. Zou, Y. Zhang, L.T. Guo, P.H. Wang, X. He, G.Z. Dai, H.W. Zheng, C.Y. Chen, A.C. Wang, C. Xu, Z.L. Wang, Quantifying the triboelectric series, Nat. Commun. 10 (2019) 1427.
[30] T. Lee, I. Kim, D. Kim, Flexible hybrid nanogenerator for self-powered weather and healthcare monitoring sensor, Adv. Electron. Mater. 7 (2021), 2100785.
[31] X.Y. Yang, G.Q. Liu, Q.Y. Guo, H.Y. Wen, R.Y. Huang, X.H. Meng, J.L. Duan, Q. W. Tang, Triboelectric sensor array for internet of things based smart traffic monitoring and management system, Nano Energy 92 (2022), 106757.
[32] R.R. Cao, Y.F. Xia, J. Wang, X.Y. Jia, C.Y. Jia, S.L. Zhu, W.F. Zhang, X.F. Gao, X. X. Zhang, Suppressing thermal negative effect and maintaining high-temperature steady electrical performance of triboelectric nanogenerators by employing phase change material, ACS Appl. Mater. Inter. 13 (2021) 41657–41668.
[33] K.M. Shi, H.Y. Zou, B. Sun, P.K. Jiang, J.L. He, X.Y. Huang, Dielectric modulated cellulose paper/PDMS-based triboelectric nanogenerators for wireless transmission and electropolymerization applications, Adv. Funct. Mater. 30 (2019), 1904536.
[34] J.W. Lee, H. Cho, J.J. Chun, K.N. Kim, S. Kim, C.W. Ahn, I.W. Kim, J.-Y. Kim, S.-W. Kim, C. Yang, J.M. Baik, Robust nanogenerators based on graft copolymers via control of dielectrics for remarkable output power enhancement, Sci. Adv. 3 (2017), e1602902.
[35] W.C. Wang, J.W. Zhang, Y.J. Zhang, F.Q. Chen, H.Y. Wang, M.J. Wu, H. Lin, Q. Y. Zhu, H.W. Zheng, R.Y. Zhang, Remarkably enhanced hybrid piezo/triboelectric nanogenerator via rational modulation of piezoelectric and dielectric properties for self-powered electronics, Appl. Phys. Lett. 116 (2020), 023901.
[36] T.P. Mena, Sutrisno, S. Marfu'ah, Antibacterial activity of free fatty acids, potassium soap, and fatty acids methyl esters from VCO (virgin coconut oil), 2nd International Conference on Chemistry and Material Science (IC2MS) 833 (2020) 012023.
[37] M.I. Fitranda, Sutrisno, S. Marfu'ah, Physicochemical properties and antibacterial activity of castor oil and its derivatives, 2nd International Conference on Chemistry and Material Science (IC2MS) 833 (2020) 012009.
[38] T. Wallek, J. Rarey, J.O. Metzger, J. Gmehling, Estimation of pure-component properties of biodiesel-related components: fatty acid methyl esters, fatty acids, and triglycerides, Ind. Eng. Chem. Res. 52 (2013) 16966–16978.
[39] K. Bober, R_M values application for calculation and prediction of selected physicochemical properties of homologous series of saturated fatty acids, J. Liq. Chromatogr. R. T 31 (2008) 567–577.
[40] S.Q. Lin, L. Xu, C. Xu, X.Y. Chen, A.C. Wang, B.B. Zhang, P. Lin, Y. Yang, H.B. Zhao, Z.L. Wang, Electron transfer in nanoscale contact electrification: Effect of temperature in the metal-dielectric cas, Adv. Mater. 31 (2019), 1808197.
[41] C.J. Lee, A.Y. Choi, C. Choi, H.J. Sim, S.J. Kim, Y.T. Kim, Triboelectric generator for wearable devices fabricated using a casting method, RSC Adv. 6 (2016) 10094–10098.
[42] L.L. Zhou, D. Liu, Z.H. Zhao, S.X. Li, Y.B. Liu, Y.K. Gao, Z.L. Wang, J. Wang, Simultaneously enhancing power density and durability of sliding-mode triboelectric nanogenerator via interface liquid lubrication, Adv. Energy Mater. 10 (2020), 2002920.
[43] A.C. Wang, B.B. Zhang, C. Xu, H.Y. Zou, Z.Q. Lin, Z.L. Wang, Unraveling temperature-dependent contact electrification between sliding-mode triboelectric pairs, Adv. Funct. Mater. 30 (2020), 1909384.
[44] C. Xu, A.C. Wang, H.Y. Zou, B.B. Zhang, C.L. Zhang, Y.L. Zi, L. Pan, P.H. Wang, P. Z. Feng, Z.Q. Lin, Z.L. Wang, Raising the working temperature of a triboelectric nanogenerator by quenching down electron thermionic emission in contact-electrification, Adv. Mater. 30 (2018), 1803968.
[45] X.K. Xie, Y. Zhang, C. Chen, X.P. Chen, T. Yao, M.F. Peng, X.J. Chen, B.Q. Nie, Z. Wen, X.H. Sun, Frequency-independent self-powered sensing based on capacitive impedance matching effect of triboelectric nanogenerator, Nano Energy 65 (2019), 103984.
[46] R.R. Bao, J. Tao, C.F. Pan, Z.L. Wang, Piezophototronic effect in nanosensors, Small Sci. 1 (2021), 2000060.
[47] X. Han, Z.S. Xu, W.Q. Wu, X.H. Liu, P.G. Yan, C.F. Pan, Recent progress in optoelectronic synapses for artificial visual-perception system, Small Struct. (2020), 2000029.
[48] G. Ge, Y. Lu, X.Y. Qu, W. Zhao, Y.F. Ren, W.J. Wang, Q. Wang, W. Huang, X. C. Dong, Muscle-inspired self-healing hydrogels for strain and temperature sensor, ACS Nano 14 (2020) 218–228.

Shaowei Shen received his B.S. from Dalian University of Technology in 2020. Now he is a M.S. student in the Henan Key Laboratory of Photovoltaic Materials at Henan University. His research focuses on environmental energy harvesting and devices.

Yangjiu Zhao received his B.S. from Henan University in 2021. Now he is a M.S. student in the Henan Key Laboratory of Photovoltaic Materials at Henan University. His current study mainly focuses on the high-temperature energy harvesting and self-powered sensor.

Dr. Ruirui Cao is currently an associate Professor in the Henan Key Laboratory of Photovoltaic Materials at Henan University. She received her Ph.D. from School of Material Science and Engineering of Tiangong University in 2019, and then, joined the Henan Key Laboratory of Photovoltaic Materials, Henan University. Her research focuses on energy conversion and storage, self-powered sensing and flexible electronic devices.

Haoyi Wu received his B.S. from Henan University Minsheng College in 2022. Now he is a M.S. student in the Henan Key Laboratory of Photovoltaic Materials at Henan University. His research focuses on wearable thermal-mechanical energy harvesting devices.

Prof. Weifeng Zhang is now a professor in the Henan Key Laboratory of Photovoltaic Materials at Henan University. He received his Ph.D. degree in Condensed Matter Physics, Nanjing University in 2000. From 2004–2006, he worked as a postdoctoral fellow in the National Institute for Materials Science, Japan. In 2010, he was elected a distinguished professor of Henan province. His research group focuses on photoelectric properties study of wide bandgap semiconductor materials, new energy conversion and storage devices.

Yuxuan Zhu received her B.S. from Panzhihua University in 2019. At present, she is pursuing her M.S. at College of Chemical Engineering, Inner Mongolia University of Technology and joint-training in Beijing Institute of Nanoenergy and Nanosystem, Chinese Academy of Sciences. Her research interest covers the application of flexible piezoelectric nanogenerators in wearable devices.

Kailiang Ren obtained his M.S. and Ph.D. degree from the Pennsylvania State University in 2005 and 2007, respectively. He was a postdoctoral fellow at the Pennsylvania State University from 2009 to 2010 and Johns Hopkins University from 2011 to 2014. Currently, he is a professor at Beijing Institute of Nanoenergy and Nanosystems. His primary research interests focus on device applications of novel electronic materials, especially soft electronic materials and ferroelectric-based materials, which include piezoelectric nanofiber based nanogenerators, energy devices for electrical energy storage and conversion, and MEMs sensors.

Dr. Caofeng Pan received his B.S. degree (2005) and his Ph.D. (2010) in Materials Science and Engineering from Tsinghua University, China. He then joined the Georgia Institute of Technology as a postdoctoral fellow. He is currently a professor and a group leader at Beijing Institute of Nanoenergy and Nanosystems, Chinese Academy of Sciences since 2013. His main research interests focus on the fields of low dimensional materials for fabricating smart electronic and optoelectronic devices for tactile sensing.